



Original Research Genitourinary and Gynecologic Imaging

Iodine quantification of renal lesions: Preliminary results using spectral-based material extraction on photon-counting CT

Adrienn Tóth¹, Jordan H. Chamberlin¹, Salvador Mendez¹, Akos Varga-Szemes¹, Andrew D. Hardie¹

¹Department of Radiology and Radiological Science, Medical University of South Carolina, Charleston, South Carolina, United States.



***Corresponding author:**
Andrew Dean Hardie,
Department of Radiology and
Radiological Science, Medical
University of South Carolina,
Charleston, South Carolina,
United States.

hardie@musc.edu

Received: 02 January 2024
Accepted: 13 January 2024
Published: 08 March 2024

DOI
10.25259/JCIS_1_2024

Quick Response Code:



ABSTRACT

Objectives: To assess the range of quantitative iodine values in renal cysts (RC) (with a few renal neoplasms [RNs] as a comparison) to develop an expected range of values for RC that can be used in future studies for their differentiation.

Material and Methods: Consecutive patients ($n = 140$) with renal lesions who had undergone abdominal examination on a clinical photon-counting computed tomography (PCCT) were retrospectively included. Automated iodine quantification maps were reconstructed, and region of interest (ROI) measurements of iodine concentration (IC) (mg/cm^3) were performed on whole renal lesions. In addition, for heterogeneous lesions, a secondary ROI was placed on the area most suspicious for malignancy. The discriminatory values of minimum, maximum, mean, and standard deviation for IC were compared using simple logistic regression and receiver operating characteristic curves (area under the curve [AUC]).

Results: A total of 259 renal lesions (243 RC and 16 RN) were analyzed. There were significant differences between RC and RN for all IC measures with the best-performing metrics being mean and maximum IC of the entire lesion ROI (AUC 0.912 and 0.917, respectively) but also mean and minimum IC of the most suspicious area in heterogeneous lesions (AUC 0.983 and 0.992, respectively). Most RC fell within a range of low measured iodine values although a few had higher values.

Conclusion: Automated iodine quantification maps reconstructed from clinical PCCT have a high diagnostic ability to differentiate RCs and neoplasms. The data from this pilot study can be used to help establish quantitative values for clinical differentiation of renal lesions.

Keywords: Photon-counting computed tomography, Iodine quantification, Renal lesion

INTRODUCTION

Photon-counting computed tomography (PCCT) was introduced into clinical practice in 2021, representing a promising technological innovation and potential to improve computed tomography (CT) imaging.^[1-5] The new detector design of PCCT employs a semiconductor material (cadmium telluride), which directly converts X-ray photons into electrical signals, and bins the incoming photons based on their energy using energy thresholds.^[6] Such spectral separation and imaging enable the generation of spectral reconstructions like iodine maps from every routine abdominal scan.^[5]

This is an open-access article distributed under the terms of the Creative Commons Attribution-Non Commercial-Share Alike 4.0 License, which allows others to remix, transform, and build upon the work non-commercially, as long as the author is credited and the new creations are licensed under the identical terms.

©2024 Published by Scientific Scholar on behalf of Journal of Clinical Imaging Science

With the increasing number of CT scans performed each year, radiologists face the diagnostic challenge to distinguish potentially malignant lesions from the large number of benign lesions incidentally detected. The standard method to characterize a renal lesion by CT imaging is to measure the increase in attenuation of the lesion between the unenhanced and contrast-enhanced phases; however, the majority of studies are not performed in two phases, more often only post-contrast. Further, although renal lesions are traditionally classified as “enhancing” when there is an increase in attenuation <20 Hounsfield units from unenhanced to contrast-enhanced phases, this method is not always reliable, particularly with modern CT scanning techniques.^[7] However, both dual-energy CT (DECT) and PCCT offer the ability to create material-specific datasets (such as iodine maps) through material decomposition, facilitating the direct quantification of iodine uptake in renal lesions. The iodine quantification with DECT has previously been proven to be an accurate and superior imaging technique for distinguishing enhancing from non-enhancing renal lesions compared to standard enhancement measurements. However, due to the inherent limitations of DECT techniques, a single universal iodine concentration (IC) threshold has not been able to be established, particularly as the threshold can vary depending on the specific DECT methodology.^[8,9] PCCT may have the potential to reduce the inherent variability seen with DECT ICs and thus more likely to perform better clinically in separating non-enhancing renal lesions from enhancing without the necessity of pre- and post-contrast phases. Therefore, the aim of this study was to assess the range of values for IC by PCCT when evaluating renal cyst (RC) and renal neoplasm (RN). Further, a preliminary assessment was performed for discrimination between RC and RN and to help establish the acceptable quantitative range of IC values, particularly for non-enhancing RCs.

MATERIAL AND METHODS

Study cohort

This retrospective, single-center, case-control study was approved by the Institutional Review Board at the Medical University of South Carolina (number Pro00131773, dated 9/18/2023). The need for written informed consent was waived due to the retrospective study design. Patients 18 years of age or older who had previously undergone abdominal CT on a first-generation dual-source PCCT scanner (NAEOTOM Alpha, Siemens Healthcare) from March to August 2023 were retrospectively included. A search of the picture-archiving communication system yielded 729 patients who underwent computed tomography of the abdomen. The type of the lesion (RC or RN) was confirmed with one of the following imaging criteria: documented enhancement on magnetic resonance imaging (MRI) or CT pre- and post-contrast

(RN) or non-enhancement (RC) and additionally for RC at least 1 year stability on prior imaging (MRI, CT, positron emission (PET) and ultrasound) or stability on two or more examinations within one year if the imaging features were considered diagnostic of a cyst. Patients were excluded from the study if no renal lesion was present ($n = 394$), the type of the lesion could not be confirmed with one of the previously detailed imaging criteria ($n = 179$ non-enhancing lesion reported as simple cyst, $n = 3$ reported as angiomyolipoma, $n = 8$ enhancing lesion suspicious for neoplasm), or if the lesion was characterized as angiomyolipoma by the presence of macroscopic fat ($n = 5$). 140 patients with 259 renal lesions constituted the final study cohort [Figure 1].

Image acquisition

Images were acquired on a clinical first-generation dual-source PCCT scanner (NAEOTOM Alpha, Siemens Healthineers, Forchheim, Germany) in the multi energy (QuantumPlus) acquisition mode at 120 kVp and an image quality level of 249. The following scan parameters were used: detector collimation 144×3 mm, pitch 0.8, gantry rotation time 0.5 s, and matrix size 512×512 . All images were obtained with automated tube current modulation (CARE Dose4D, Siemens Healthcare).

Iodine quantification maps were automatically reconstructed for each scan from axial images and were displayed in grayscale. In brief, photon-counting detectors distinguish between different materials, such as iodine and surrounding tissues, by measuring the energy of individual photons and sorting them into different energy bins. Material decomposition algorithms utilize energy information and unique energy attenuation characteristics to estimate the concentrations of various materials in each voxel of the CT volume. This results in the synthesis of material-specific density maps with pixel values expressed in mg/cm^3 .

Abdominal CT indications included staging and evaluation of already known oncologic disease ($n = 75$), non-traumatic abdominal emergencies ($n = 46$), surgical consultation or postoperative complications ($n = 18$), and urinary symptoms ($n = 1$). The imaging protocol varied among the patients, including single portal venous phase ($n = 112$), biphasic ($n = 20$), four-phase protocol ($n = 7$), and CT urography with nephrogenic and excretory phase ($n = 1$). A weight-adapted intravenous iodinated contrast agent containing 350 mg of iodine per mL (iohexol, Omnipaque™ 350, GE Healthcare) at an average dose of $1.25 (\pm 0.13)$ mL/kg of body weight at a flow rate of $2.96 (\pm 0.59)$ mL/s was injected.

Image analysis

Regions of interest (ROIs) were manually placed by one reader on the generated iodine quantification maps. The ROIs were

placed in the interior of the renal lesion, as large as possible to cover the entire lesion, as close to the lesion border as possible, but without crossing the edges. For each lesion, the minimum, maximum, mean, and standard deviation (SD) of the IC (in

mg/cm³) were recorded. The type of lesion, location (left/right kidney, upper/middle/lower pole), size (3 dimensions), and position (endophytic/exophytic) were recorded for each lesion. For each patient, up to three lesions were measured (largest,

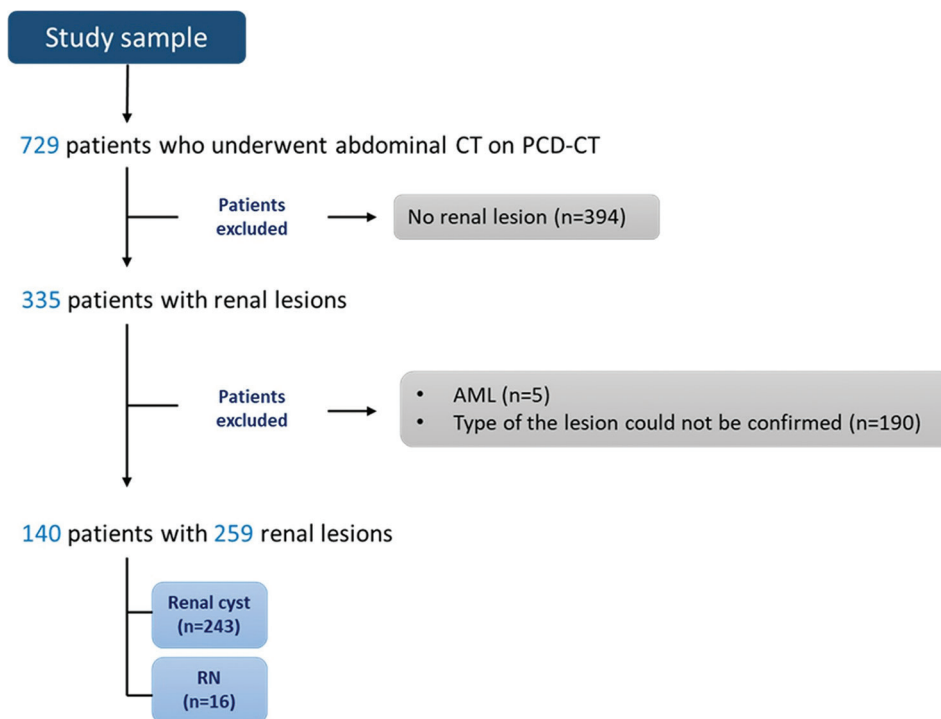


Figure 1: Study population. (AML: Angiomyolipoma, CT: Computed tomography, n: Number, PCD-CT: Photon-counting detector computed tomography, RN: Renal neoplasm).



Figure 2: (a) A 86-year-old female who presented with abdominal pain. Reconstructed iodine quantification map of the axial CT image shows the left kidney with renal cyst. For homogeneous lesions, one ROI was placed in the interior of the renal lesion, as large as possible to cover the entire lesion (yellow arrow pointing to the ROI shown as yellow circle). (b) A 64-year-old female presented for RCC staging. A reconstructed iodine quantification map of the axial CT image shows the right kidney with renal neoplasm. For heterogeneous lesions, after the placement of the first ROI (yellow arrow pointing to the ROI shown as yellow circle), a secondary ROI (yellow star marking the ROI shown as yellow circle) was placed on the area of the highest conspicuity of iodine concentration. (CT: Computed tomography, RCC: Renal cell carcinoma, ROI: Region of interest).

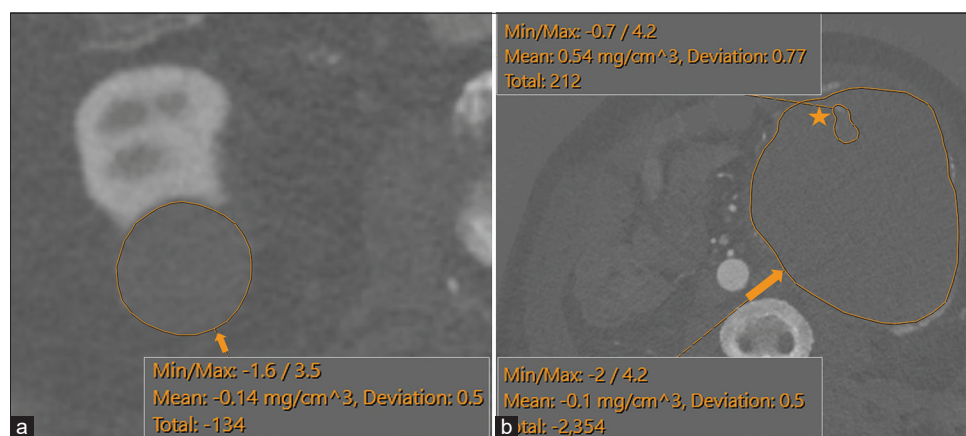


Figure 3: (a) A 78-year-old male presented with angiosarcoma of the scalp for staging. A reconstructed iodine quantification map of the axial CT image shows the right kidney with a renal cyst, showing an unusually high maximum IC (yellow arrow pointing to the ROI covering the entire lesion, shown as a yellow circle). This lesion was subsequently reviewed and confirmed to be a renal cyst. (b) A 67-year-old male presented with metastatic RCC for staging. Reconstructed iodine quantification map of axial CT image shows left kidney with RN. For heterogeneous lesions, after the placement of the first ROI (yellow arrow pointing to the ROI shown as yellow circle), a secondary ROI (yellow star marking the ROI shown as yellow circle) was placed on the area of the highest conspicuity of IC. This RN fell within a lower range of IC and was subsequently reviewed and determined to have previously received chemotherapy, indicating a likelihood of reduced vascularity. (CT: Computed tomography, IC: Iodine concentration, RCC: Renal cell carcinoma, RN: Renal neoplasm, ROI: Region of interest).

medium, and smallest). For heterogeneous (non-uniform) lesions, a secondary ROI of variable size was placed on the area of the highest conspicuity of IC and used for secondary analysis [Figures 2 and 3]. For homogeneous lesions, the first ROI was used in place of the secondary ROI during analysis.

Statistical analysis

Post hoc power analysis was performed using the observed effect size of the mean iodine density as a benchmark due to the lack of prior literature data on the expected effect size for spectral quantification. The observed power for differences in mean IC by the two-sided Mann-Whitney U test was 0.98. Medians and interquartile ranges were calculated for all continuous variables and frequency data for categorical variables. All variables were assessed for a pattern of distribution using histograms. Using simple logistic regression, paired receiver operating characteristic (ROC) curves were constructed and the area under the curve (AUC) was calculated with confidence intervals by DeLong's method. All data analyses were performed in R version 4.1.2 (R Foundation for Statistical Computing, Vienna, Austria).

RESULTS

Among the 140 patients, abdominal CT indications included staging and evaluation of already known oncologic disease ($n = 75$), non-traumatic abdominal emergencies ($n = 46$), surgical consultation or postoperative complications ($n = 18$), and urinary symptoms ($n = 1$). There were 53 females (37.8%)

and 87 males (62.1%) with an aggregate mean age of 66 ± 12 years. Radiation dose parameters were as follows: effective mAs 184.9 ± 77.3 , volume CT dose index 15.2 ± 6.6 mGy, dose length product 1020.5 ± 608.0 mGy*cm, and size-specific dose estimate 18.3 ± 5.9 mGy.

A total of 259 lesions (16 RNs and 243 cysts) were included in the final analysis [Figure 1]. There was no statistically significant difference in laterality ($P = 0.358$), location within the kidney ($P = 0.054$), or minimum IC of the entire lesion ($P = 0.074$). RNs were found to be larger (21.2 ± 190 mL vs. 0.8 ± 3.4 mL, $P < 0.001$) and were more likely to be exophytic (56.2% vs. 26.3%, $P = 0.022$) [Table 1].

Whole lesion mean IC was 1.3 ± 2.3 mg/cm³ for RNs and 0 ± 0.3 mg/cm³ for cysts ($P < 0.001$). There was a statistically significant increase in maximum whole lesion IC for RNs versus cysts (5.3 ± 3.3 mg/cm³ vs. 1.4 ± 0.8 mg/cm³, $P < 0.001$). There was no difference in minimum IC. RNs also were statistically more heterogeneous with an increase in the SD of IC across the whole lesion (0.9 ± 0.7 vs. 0.5 ± 0.2 , $P < 0.001$) [Table 1]. Distributions of the respective variables are given in Figure 4, which demonstrates that cysts have a relatively narrow window of possible IC, while RN IC was more heterogeneous and positively skewed.

A second ROI representing the subjective area of the highest IC was measured. The mean, maximum, minimum, and SD of this IC for the select ROI were statistically higher in comparison to the measurement of the whole lesion ($P = 0.002$, 0.006, 0.002, and 0.002, respectively) [Table 2 and Figure 4].

Table 1: Characteristics of renal lesions stratified by etiology per imaging criteria.

<i>n</i> =259	RN (<i>n</i> =16)		RC (<i>n</i> =243)		<i>P</i> -value
	<i>n</i> (%) Median (IQR)		<i>n</i> (%) Median (IQR)		
Laterality					
Left	10 (62.5)		115 (47.3)		0.358
Right	6 (37.5)		128 (52.7)		
Location					
Superior Pole	8 (50.0)		67 (27.6)		0.054
Mid-Pole	2 (12.5)		99 (40.7)		
Inferior Pole	6 (37.5)		77 (31.7)		
Position					
Exophytic	9 (56.2)		64 (26.3)		0.022
Endophytic	7 (43.8)		179 (73.7)		
Max Dimension (mm)	34.4 (51.2)		11.7 (11.3)		<0.001
Volume (mL)	21.2 (190.6)		0.8 (3.4)		<0.001
Mean Iodine (mg/cm ³)	1.3 (2.3)		0 (0.3)		<0.001
Minimum Iodine (mg/cm ³)	-0.7 (1.1)		-1.2 (0.7)		0.074
Maximum Iodine (mg/cm ³)	5.3 (3.3)		1.4 (0.8)		<0.001
SD Iodine	0.9 (0.7)		0.5 (0.2)		<0.001

Bold values denote statistical significance at the *P* < 0.05 level. IQR: Interquartile range, *n*: Number, RC: Renal cyst, RN: Renal neoplasm, SD: Standard deviation

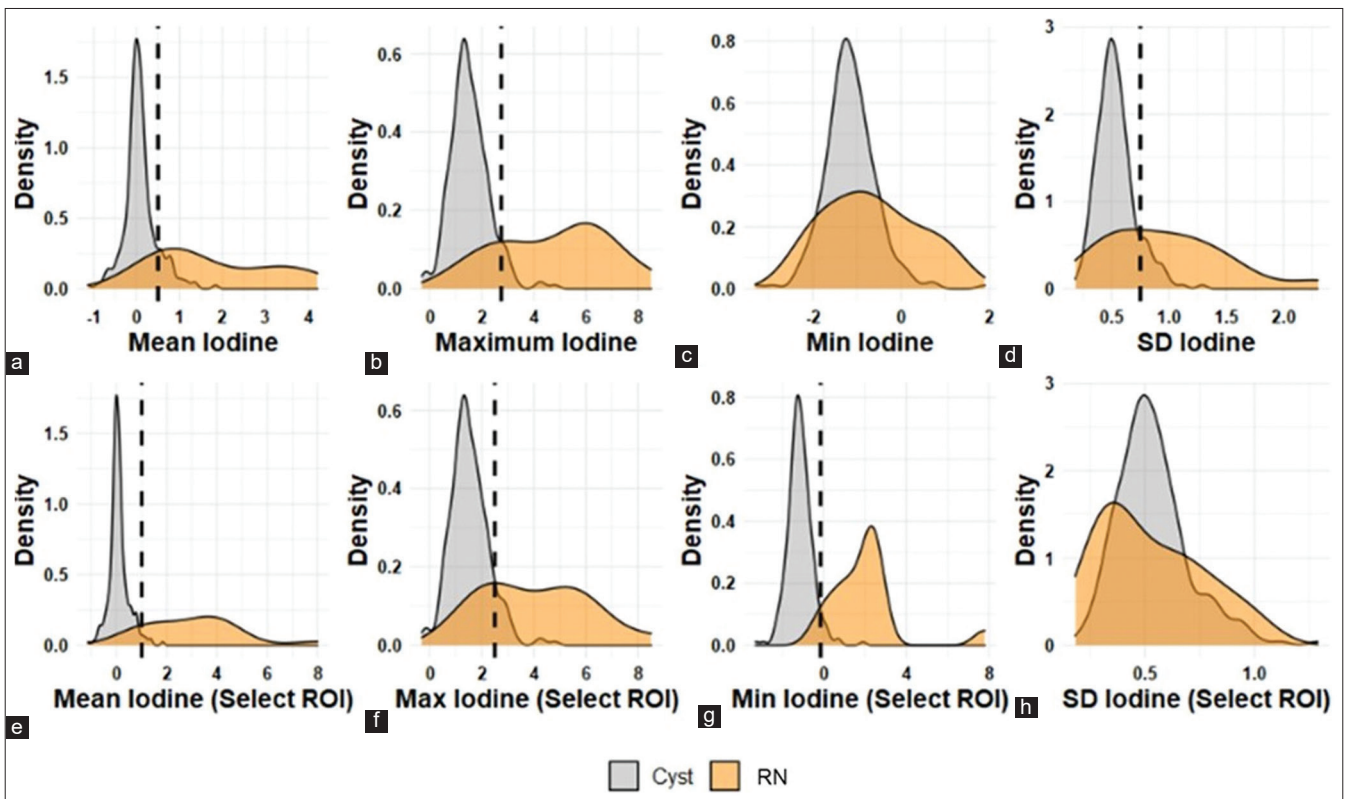


Figure 4: Comparison of the distributions of iodine measurements stratified by lesion type. (a-d): Graphs show the distribution of the mean (a), maximum (b), minimum (c) iodine and standard deviation (d) measurements in the ROIs covering the entire lesion. (e-f): Graphs show the distribution of the mean (e), maximum (f), minimum (g) iodine and standard deviation (h) measurements in the select ROIs placed on the area of the highest conspicuity of iodine concentration. Cysts had narrowly distributed iodine concentrations, whereas RN had more complex heterogeneous distributions with positive skew. (RN: Renal neoplasm, ROI: Region of interest, SD: Standard deviation).

Table 2: Comparison of ROI measurements for the whole lesion and the secondary ROI for the most enhancing component.

	ROI 1 (Whole Lesion)	ROI 2 (Most Enhancing)	P-value
	Median (IQR)	Median (IQR)	
Mean Iodine (mg/cm ³)	1.3 (2.3)	3.3 (2.6)	0.002
Maximum Iodine (mg/cm ³)	5.3 (3.3)	4.1 (3.4)	0.006
Minimum Iodine (mg/cm ³)	-0.7 (1.1)	2.2 (1.4)	0.002
SD Iodine	0.9 (0.7)	0.5 (0.3)	0.002

ROI: Region of interest, SD: Standard deviation, IQR: Interquartile range

Table 3: Comparison of ROC curves for each measurement stratified by region of interest.

n=16 RN, n=243 RC	ROI 1 (Whole Lesion)	ROI 2 (Most Enhancing)	P-value (ROI 1:2)
	AUC (95% CI)	AUC (95% CI)	
Mean Iodine	0.912 (0.822–1)	0.983 (0.961–1)	0.146
Maximum Iodine	0.917 (0.820–1)	0.890 (0.791–0.990)	0.075
Minimum Iodine	0.633 (0.444–0.822)	0.992 (0.981–1)	0.001
SD Iodine	0.768 (0.600–0.936)	0.543 (0.350–0.737)	0.155

Bold values denote statistical significance at the $P < 0.05$ level. AUC: Area under the curve, CI: Confidence interval, n: Number, RC: Renal cyst, RN: Renal neoplasm, ROC: Receiver operating characteristic, ROI: Region of interest, SD: Standard deviation

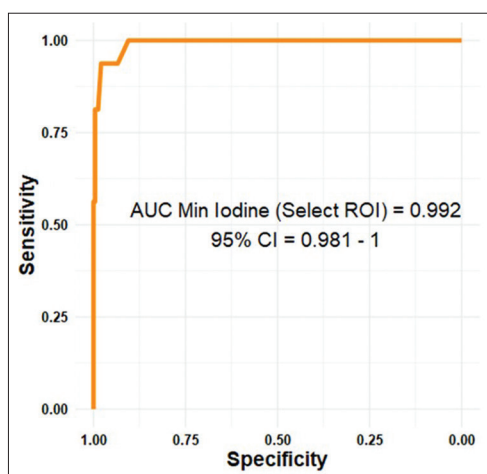


Figure 5: ROC curve for the prediction of lesion type by minimum iodine concentration of the selected ROI. AUC of the minimum iodine concentration for the area of greatest enhancement = 0.992 (95% CI 0.981–1). (AUC: Area under the curve, CI: Confidence interval, ROC: Receiver operating characteristic, ROI: Region of interest).

The explanatory capability of each measurement for the differentiation of RN and cyst was performed using ROC analysis via simple logistic regression. Among whole lesion large ROI measurements, the mean and maximum ICs were found to be most predictive (mean IC AUC = 0.912; 95% confidence interval [CI]: 0.822–1; maximum IC AUC = 0.917; 95% CI: 0.820–1). Regarding selected ROIs of the area of most conspicuity, both mean IC and minimum IC performed near perfectly (mean IC AUC = 0.983; 95% CI: 0.961–1;

minimum IC AUC = 0.992; 95% CI: 0.981–1) [Table 3 and Figure 5].

DISCUSSION

Overall, the spectral-based material extraction by PCCT for the measurement of the IC in renal lesions on the reconstructed iodine quantification maps had a high diagnostic ability to differentiate RCs and RNs. More essentially, the range of IC values for RC clustered at the lowest IC values. Interestingly, the only RN that fell within this lower range was subsequently reviewed and determined to have previously received chemotherapy, indicating a likelihood of reduced vascularity which could explain the low IC value. Thus, for this preliminary study, the results provide a meaningful reference for future studies regarding the range of IC of “non-enhancing” renal lesions. For data collected on the mean, minimum, and maximum IC for homogeneous renal lesions, there were significant differences between RCs and RNs for all IC assessments (minimum, maximum, mean, and SD) with the best performing ROC curve for mean IC (AUC 0.983) and minimum IC (AUC 0.992). RNs had quantitatively higher concentrations with biologically plausible thresholds for measurement. For instance, cysts rarely had whole lesion mean ICs > 0.5 or maximum concentrations > 3. Regarding the most conspicuous ROI measurements, cysts seldom had a minimum IC > 0, while RNs seldom had measurements < 0. Hence, this simple and easily applicable quantitative methodology allows for a generalizable application of ROI placement and assessment of IC to evaluate lesion vasculature.

Related literature on iodine quantification of renal lesions by CT has been limited to energy-integrating detector (EID) CT platforms.^[8-14] Ascenti *et al.* assessed the diagnostic accuracy of dual-source dual-energy CT-based iodine quantification.^[8] The authors reported that iodine quantification was more accurate than standard enhancement measurements when the ROI covered the entire lesion, and noted that the presence of the iodine in renal masses could be considered as representative of vascularity. Marin *et al.* reported similar results when assessing the diagnostic accuracy of iodine quantification for the detection of small (1–4 cm) renal lesions using a rapid kilovolt-switching single-source multidetector row CT system.^[10] According to their results, single-phase contrast-enhanced dual-energy material attenuation analysis showed improved specificity for the characterization of small renal lesions using an iodine-water concentration threshold of 1.9 mg/cm³. This improvement was attributed to the reduced number of false-positive findings due to pseudoenhancement.

A recent study by Sartoretti *et al.* revealed that PCCT matches the overall performance of EID-CT in iodine quantification and delivers accurate results independent of radiation dose, IC, and base material attenuation.^[15] With PCCT, the reconstruction of iodine maps is available on every routinely performed abdominal scan, without the need for prior, user-dependent selection of dual-energy protocol. Vrbaski *et al.* found similar results investigating the potential of PCCT for low-dose quantitative spectral tasks in a recent phantom study. They reported comparable iodine quantification accuracy between standard and low radiation doses on PCCT when outperforming accuracy on dual-energy CT.^[16]

The authors argue that the observed distribution of IC matches the known pathophysiology of renal lesions. Cysts exhibited a very narrow range of iodine values, with mean values falling in a predictable distribution centered around zero iodine. Maximum values were predictably higher in RNs than they were in cysts. Most importantly, the minimum IC of the most suspicious area was seldom less than zero, and conversely, minimum values for cysts were seldom greater than zero. This dichotomy is stark evidence for the pathophysiology at hand – neoplasms are abnormally vascular structures and cysts are not. The fact that the minimum IC of the whole lesion was unrevealing is also important as this demonstrates the concept that neoplasms are heterogeneous and can have avascular components, a conclusion that is bolstered by the observed variance data in this study.

Large, heterogeneous renal masses do not represent a diagnostic dilemma on routine CT. The value of PCCT may be better demonstrated by distinguishing complicated cysts from smaller, more homogeneous, or hypovascular solid masses. However, it is important to establish the general utility of this technique and determine appropriate cutoff thresholds before using it for more specific applications. Due to the high frequency of renal

lesions in adult CT scans, it is essential to have a technique that can accurately identify benign cysts during the initial incidental encounter. PCCT offers a direct means to assess lesion vascularity in a single acquisition, which can save time and resources by avoiding unnecessary follow-up examinations. The study evaluated the accuracy of iodine quantification through PCCT, contributing to the development of this emerging technology.

Limitations of our study merit consideration. First, our study population had a relatively lower number of RNs. This imbalance may affect the validity of parameters such as AUC, potentially not accurately reflecting the actual diagnostic performance. In addition, the full range of IC values in RNs may not have been fully assessed in this preliminary study, and further studies need to be carried out in a more diverse population and evaluate different types of RNs. Second, follow-up imaging was used as the confirmation method of the type of renal lesions, and histopathological proof was not obtained. It is known that some RCCs progress very slowly in their early stages; thus, stability in size does not necessarily mean it is benign. However, this method is common for such analyses, as cysts are seldom excised.^[11,17] Only including lesions with follow-up histological proof (that are not clearly benign on CT) would have been biased toward complicated cysts. Third, the large number of non-confirmed lesions during the enrollment process and the high number of known oncologic disease indications could potentially introduce significant selection bias. Finally, only one reader obtained the objective measurements, which could be considered a weakness of the study design as it limits the generalizability of our study results. However, ROIs of various lesions are routinely acquired in practice and have extensive bodies of literature about interrater reliability. To avoid potential misinterpretation of preliminary datasets, reader agreement or reproducibility was not assessed in our study.

CONCLUSION

This study provides useful preliminary data regarding the range and upper limit of the IC of “non-enhancing” renal lesions. Combined with future work, these data can be used to help establish quantitative values for the differentiation of RC and RN and provide a benchmark for future spectral analysis hypotheses.

Ethical approval

The research/study was approved by the Institutional Review Board at the Medical University of South Carolina, number Pro00131773, dated 9/18/2023.

Declaration of patient consent

The authors certify that they have obtained all appropriate patient consent forms.

Financial support and sponsorship

Nil.

Conflicts of interest

The authors disclose Andrew D. Hardie received financial considerations either ongoing or in the past from Siemens entities.

Use of artificial intelligence (AI)-assisted technology for manuscript preparation

The authors confirm that there was no use of artificial intelligence (AI)-assisted technology for assisting in the writing or editing of the manuscript and no images were manipulated using AI.

REFERENCES

- Euler A, Higashigaito K, Mergen V, Sartoretti T, Zanini B, Schmidt B, *et al.* High-pitch photon-counting detector computed tomography angiography of the aorta: Intraindividual comparison to energy-integrating detector computed tomography at equal radiation dose. *Invest Radiol* 2022;57:115-21.
- Sartoretti T, Landsmann A, Nakhostin D, Eberhard M, Roeren C, Mergen V, *et al.* Quantum iterative reconstruction for abdominal photoncounting detector CT improves image quality. *Radiology* 2022;304:E55.
- Schwartz FR, Alkadhi H. Photon-counting detector CT for abdominal imaging: Opportunities and challenges. *Eur Radiol* 2023;33:7805-6.
- Schwartz FR, Samei E, Marin D. Exploiting the potential of photon-counting CT in abdominal imaging. *Invest Radiol* 2023;58:488-98.
- Rajendran K, Petersilka M, Henning A, Shanblatt ER, Schmidt B, Flohr TG, *et al.* First clinical photon-counting detector CT system: Technical evaluation. *Radiology* 2022;303:130-8.
- Willemink MJ, Persson M, Pourmorteza A, Pelc NJ, Fleischmann D. Photon-counting CT: Technical principles and clinical prospects. *Radiology* 2018;289:293-312.
- Hardie AD, Perry JD, Bradshaw ML, Picard MM. Increased renal cyst density on abdominal CT at 100-kVp compared with 120-kVp: A preliminary evaluation. *Clin Imaging* 2015;39:642-5.
- Ascenti G, Mileto A, Krauss B, Gaeta M, Blandino A, Scribano E, *et al.* Distinguishing enhancing from nonenhancing renal masses with dual-source dual-energy CT: Iodine quantification versus standard enhancement measurements. *Eur Radiol* 2013;23:2288-95.
- Chandarana H, Megibow AJ, Cohen BA, Srinivasan R, Kim D, Leidecker C, *et al.* Iodine quantification with dual-energy CT: Phantom study and preliminary experience with renal masses. *AJR Am J Roentgenol* 2011;196:W693-700.
- Marin D, Davis D, Choudhury KR, Patel B, Gupta RT, Mileto A, *et al.* Characterization of small focal renal lesions: Diagnostic accuracy with single-phase contrast-enhanced dual-energy CT with material attenuation analysis compared with conventional attenuation measurements. *Radiology* 2017;284:737-47.
- Mileto A, Marin D, Ramirez-Giraldo JC, Scribano E, Krauss B, Mazziotti S, *et al.* Accuracy of contrast-enhanced dual-energy MDCT for the assessment of iodine uptake in renal lesions. *AJR Am J Roentgenol* 2014;202:W466-74.
- Kaza RK, Caoili EM, Cohan RH, Platt JF. Distinguishing enhancing from nonenhancing renal lesions with fast kilovoltage-switching dual-energy CT. *AJR Am J Roentgenol* 2011;197:1375-81.
- Liu X, Zhou J, Zeng MS, Ma Z, Ding Y. Homogeneous high attenuation renal cysts and solid masses--differentiation with single phase dual energy computed tomography. *Clin Radiol* 2013;68:e198-205.
- Mileto A, Marin D, Alfaro-Cordoba M, Ramirez-Giraldo JC, Eusemann CD, Scribano E, *et al.* Iodine quantification to distinguish clear cell from papillary renal cell carcinoma at dual-energy multidetector CT: A multireader diagnostic performance study. *Radiology* 2014;273:813-20.
- Sartoretti T, Mergen V, Jungblut L, Alkadhi H, Euler A. Liver iodine quantification with photon-counting detector CT: Accuracy in an abdominal phantom and feasibility in patients. *Acad Radiol* 2023;30:461-9.
- Vrbaski S, Bache S, Rajagopal J, Samei E. Quantitative performance of photon-counting CT at low dose: Virtual monochromatic imaging and iodine quantification. *Med Phys* 2023;50:5421-33.
- Schade KA, Mergen V, Sartoretti T, Alkadhi H, Euler A. Pseudoenhancement in cystic renal lesions - impact of virtual monoenergetic images of photon-counting detector CT on lesion classification. *Acad Radiol* 2023;30:S305-13.

How to cite this article: Toth A, Chamberlin JH, Mendez S, Varga-Szemes A, Hardie AD. Iodine quantification of renal lesions: Preliminary results using spectral-based material extraction on photon-counting CT. *J Clin Imaging Sci.* 2024;14:7. doi: 10.25259/JCIS_1_2024